Analyzing Mechanical Mechanisms in Forming High-Latitude Thermosphere Density and Wind Structures

Anton Buynovskiy[1], Jeffrey P. Thayer[1,2]

[1]CU Boulder/Aerospace Engineering Science, [2]CU Boulder/SWxTREC; Corresponding Author: anton.buynovskiy@colorado.edu

Motivation

- Results from CHAMP accelerometry revealed mesoscale (few thousand kilometers) mass density structures that coincided with signatures of wind influence at the high-latitude thermosphere [1]
- Co-located density and wind structures can indicate a potential relationship between mass density and winds that produce perturbations detectable by highly sensitive accelerometers
- High-latitude features (e.g., mass density cusp enhancement) are difficult to model solely considering direct energy inputs into the thermosphere [2, 3]
- This poster focuses on how mechanical mechanisms (e.g., ion drag) can distribute energy and produce mesoscale perturbations in the high-latitude mass density and wind structures

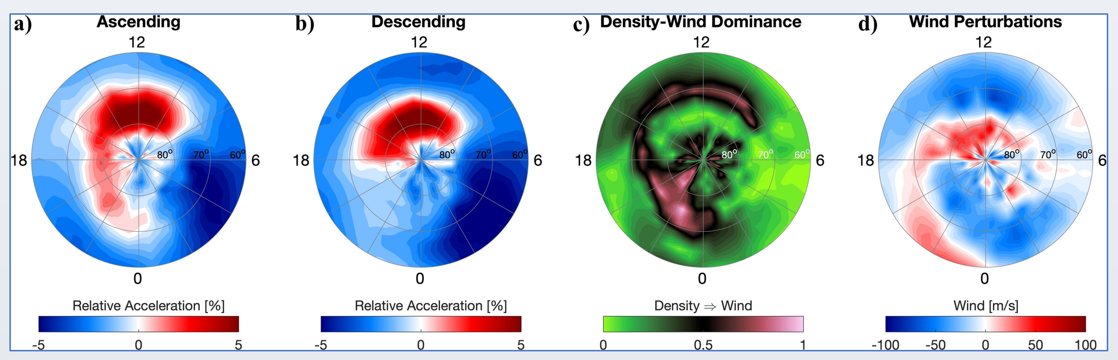

Figure 1: Results from Buynovskiy et al. (2025) demonstrating relative accelerations in the ascending and descending satellite trajectories with an analysis of density-wind dominance and detected wind perturbations

Theoretical Framework

➢ Thermosphere-Ionosphere-Electrodynamics General Circulation Model (TIEGCM)
- Physical model that self-consistently solves the 3D momentum (Eq. 1) , energy (Eq. 2), and continuity equation of the entangled ionosphere-thermosphere system and coupled with the magnetosphere [4]
- Outputs thermospheric state properties and individual heat terms, enabling a detailed energy analysis

➢ Linking the TIEGCM energy equation to thermodynamic principles
- TIEGCM's energy equation is directly mapped to the first law of thermodynamics shown (Eq. 4a)
- At 400 km, negligible eddy diffusion simplifies the energy balance to **adiabatic** (mechanical work) and **diabatic** (external heating/cooling) processes
- **Adiabatic** and **diabatic** heat terms can also be expressed using temperature, potential temperature, and vertical winds (Eq. 4b) [5]

➢ Imposing mechanical forcing in TIEGCM
- To investigate how mechanical forcing can modify the mass density and wind structures, two model scenarios are developed at analyzed constant altitude:
  - Run 1: Baseline
    - $K_p = 2$, $F_{10.7} = 150$ solar flux units, solar maximum, June solstice
  - Run 2: Increased mechanical forcing
    - Identical solar inputs as Run 1
    - The momentum equation (Eq. 1) is modified by doubling the ion drag force at high-latitudes

$$\frac{\partial v_n}{\partial t} = F_{Pressure\ Gradient} + F_{Ion\ Drag} + F_{Viscous} + F_{Coriolis} + F_{Advection} + F_{Other} \quad \cdots\cdots \text{(Eq. 1)}$$

Negligible at 400 km

$$\frac{\partial T_n}{\partial t} = H_{Cond} + H_{Eddy\ Diff} + H_{Advec} + H_{Adiabatic} + (H_{Solar} + H_{Chem} + H_{Joule}) + H_{cool} \quad \cdots \text{(Eq. 2)}$$

Q is the sum of solar heating, joule heating, and chemistry

L is NO and CO2 cooling

$$\frac{\partial T_n}{\partial t} = \frac{ge^z}{p_0 C_p}\frac{\partial}{\partial Z}\left(\frac{K_T}{H}\frac{\partial T_n}{\partial Z}\right) - v_n \cdot \nabla T_n - W\frac{\partial T_n}{\partial Z} - W\frac{R^* T_n}{C_p \bar{m}} + \frac{Q^{exp} - e^z L^{exp}}{C_p} - L^{imp} T_n \quad \cdots\cdots\cdots \text{(Eq. 3)}$$

$$\text{(Eq. 4a)} \quad \frac{DT}{Dt} = \frac{1}{c_p}\frac{Dq}{Dt} + \frac{RT}{c_p}\frac{1}{\rho}\frac{Dp}{Dt} \quad = \quad \frac{DT}{Dt} = \left(\frac{p}{p_o}\right)^{\frac{R}{c_p}}\frac{D\theta}{Dt} + \frac{g}{c_p} w_d \quad \text{(Eq. 4b)}$$

Purple = Total temperature rate
Red =Diabatic heating rate
Blue =Adiabatic heating rate

Potential Temperature

$$\theta \equiv T_N \left(\frac{p_o}{p}\right)^{\frac{R}{c_p}}$$

Results

Demonstrating First Law of Thermodynamics Compliance

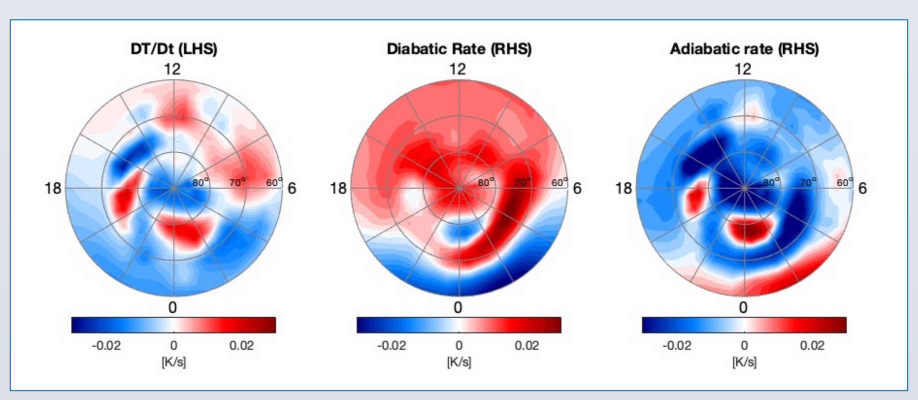

Figure 2: Validation of the first law of thermodynamics using TIEGCM energy equation terms (Eq.4a)

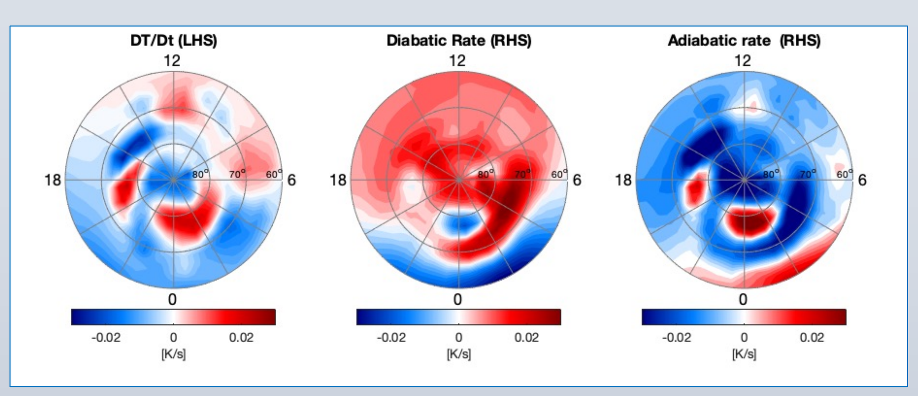

Figure 3: Validation of the first law of thermodynamics using observable-based diabatic and adiabatic heating terms (Eq. 4b)

- Figure 2 demonstrates that **TIEGCM satisfies the first law of thermodynamics**
  - Left-hand side (total temperature rate) equals the right-hand side (sum of the diabatic and adiabatic terms)
- Figure 3 shows that the **diabatic and adiabatic heating rates can be directly computed from observables**, reproducing the balance in Fig. 2
- Note: The first law of thermodynamics computes the total (material) derivatives, composed of the local time rate of change and advective terms
  - Including advective terms can make a qualitative analysis with observables difficult to interpret
  - In this analysis, the advection terms approximately cancel, which allows a reduced form of the first law as shown in Eq. 5

$$\frac{\partial T}{\partial t} \approx \left(\frac{P}{P_o}\right)^{\frac{R}{c_p}}\frac{\partial\theta}{\partial t} + \left(\frac{RT}{c_p p}\right)^{\frac{R}{c_p}}\frac{\partial p}{\partial t} \quad \cdots\cdot \text{(Eq. 5)}$$

Where T is the neutral temperature, P is the in-situ pressure, P_o is a reference pressure (1e-5 Pa for this case), θ is the potential temperature, R is the specific gas constant, and c_p is the specific heat at constant pressure

Tracking Diabatic vs Adiabatic Influence

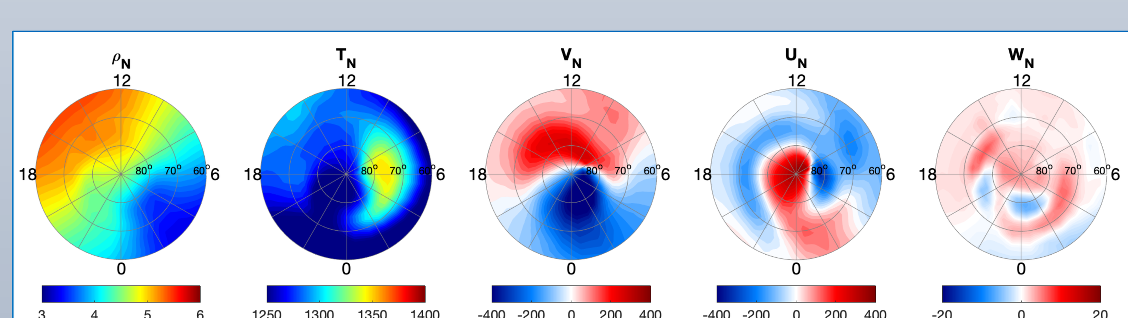

Figure 4: Thermospheric state for run 1 (baseline) at UT = 01:00

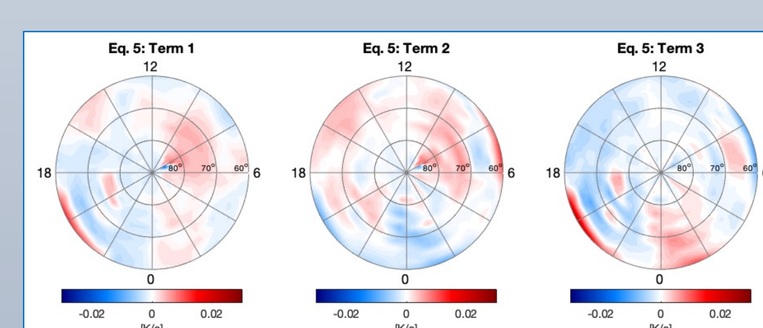

Figure 5: Reduced first law terms (Eq. 5) for run 1 at UT = 01:00

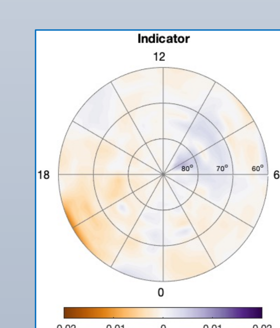

Figure 6: Run 1 diabatic vs adiabatic indicator

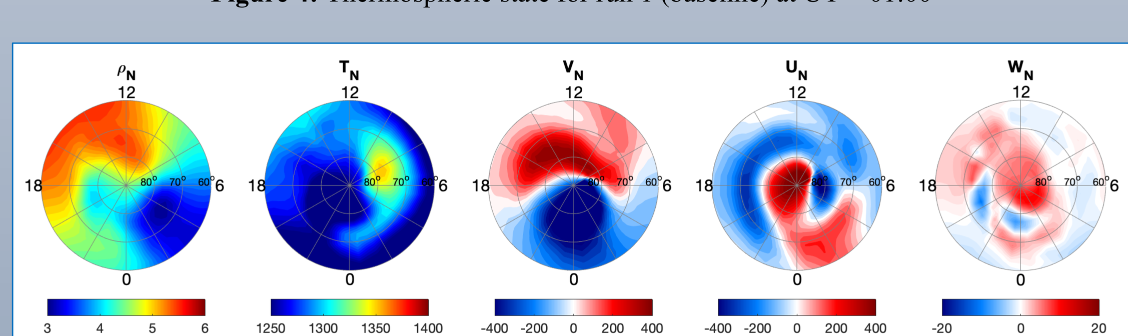

Figure 7: Thermospheric state for run 2 (enhanced ion drag) at UT = 01:00

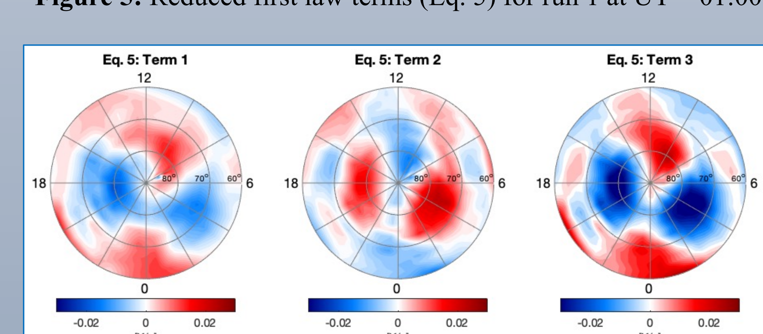

Figure 8: Reduced first law terms (Eq. 5) for run 2 at UT = 01:00

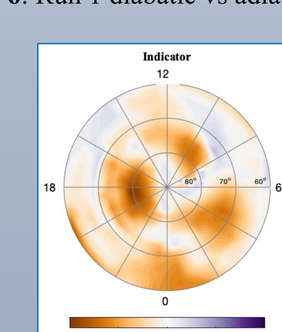

Figure 9: Run 2 diabatic vs adiabatic indicator

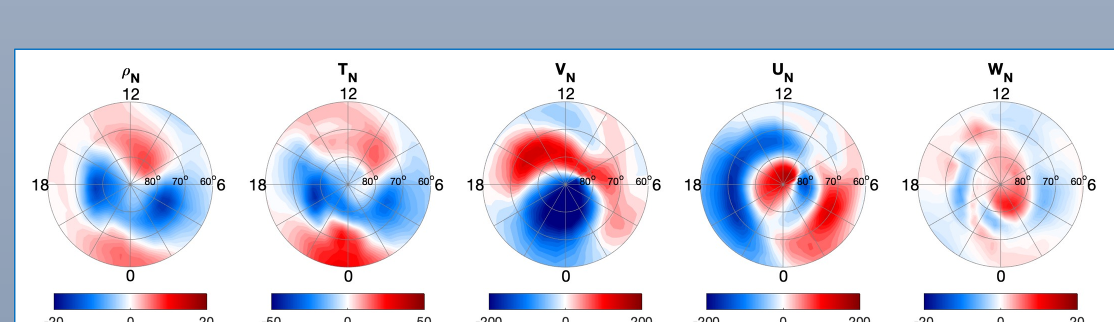

Figure 10: Thermosphere state comparison between run 1 and run 2

- Figures 4-9 illustrate the thermospheric states and corresponding diabatic/adiabatic energy contributions for runs 1 and 2 after one hour, organized in geomagnetic coordinates
- Run 1 (Fig. 4-6) show a **near steady-state system with small diabatic/adiabatic effects**
- Run 2 (Fig. 7-9) demonstrates **strong increases in diabatic/adiabatic** and **dominant adiabatic responses driven by increased ion drag**
- Figure 10 compares the thermospheric state between Runs 1 and 2, revealing **mass density changes up to 20%, temperature changes up to 50 K, and up to 200 m/s changes in the horizontal winds**

Discussion

Connecting the First Law of Thermodynamics to TIEGCM

- TIEGCM has been verified to satisfy the first law (see Fig. 2) at the high-latitude thermosphere
- Thermosphere energy exchange can be reduced to:
  - **Internal energy** changes (total temperature rate)
  - **Diabatic heating** (solar heating, joule heating, etc.)
  - **Adiabatic processes** (expansion/compression work)
- Thermosphere state variables (temperature, potential temperature, vertical winds) enable the tracking of diabatic and adiabatic contributions via Eq. 4b
  - **This framework provides a diagnostic tool to assess the drivers of energy distribution in the thermosphere without requiring the full energy equation (Eq. 3)**
  - Divergent vertical winds captures the adiabatic temperature changes due to expansion/compression without external heating
  - Potential temperature variations capture the net diabatic heating contributions

Implications Modeling and Observing Mesoscale Structures

- **The formation of mesoscale structures (e.g., neutral cusp enhancement) must consider both direct energy sources (e.g., joule heating) in addition to momentum-driven sources responsible for net adiabatic effects**
  - Figure 10 demonstrates how direct and indirect energy mechanisms can produce similar heating/cooling
- In-situ satellite measurements can track diabatic and adiabatic energy transfer using accurate measurements of few observables: pressure, temperature, and wind
  - Can help explain the underlying mechanisms responsible for the observed acceleration perturbation responses from Fig. 1

Thermosphere Response to Induced Mechanical Forcing

- Ion drag (a momentum term) was doubled in a TIEGCM simulation, producing the following changes after one hour:
  - Mass density changes up to 20%
  - Temperature changes up to 50 K
  - Horizontal wind changes up to 200 m/s
- The thermosphere response followed a self-consistent feedback:
  - Momentum forcing induced → winds respond → heating terms adjust → further dynamic response
- **Adiabatic heating/cooling can match or exceed diabatic contributions,** with a strong effect seen with a momentum-induced case study (see Figure 9 vs Figure 10)
  - Direct heat sources are not needed to significantly modulate the thermosphere mass density, temperature, and winds

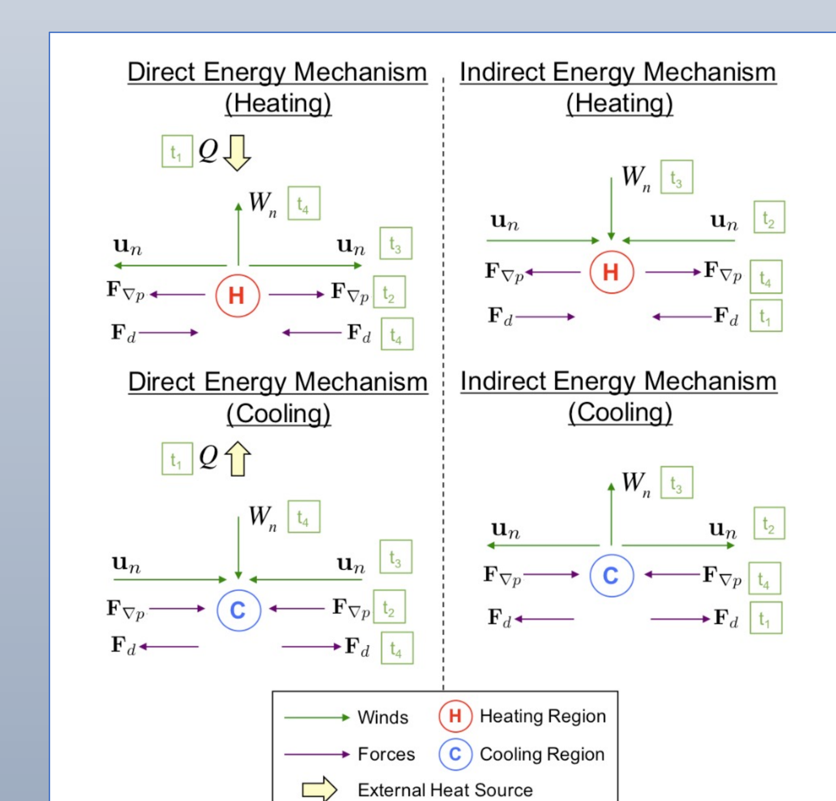

Figure 10: Direct vs indirect energy mechanisms [6]

References

1. Buynovskiy, A., Thayer, J. P., & Sutton, E. K. (2025). Mass density and wind perturbations in the high-latitude thermosphere. *Journal of Geophysical Research: Space Physics*, 130, e2025JA033910. https://doi.org/10.1029/2025JA033910 **(in production)**
2. Brinkman, D. G., Walterscheid, R. L., Clemmons, J. H., & Hecht, J. H. (2016). High-resolution modeling of the cusp density anomaly: Response to particle and Joule heating under typical conditions. *Journal of Geophysical Research: Space Physics*, **121**, 2645–2661. https://doi.org/10.1002/2015JA021658
3. Deng, Y., Fuller-Rowell, et al (2013). Theoretical study: Influence of different energy sources on the cusp neutral density enhancement. *JGR:Space Physics*, **118**, https://doi.org/10.1002/jgra.50197
4. Qian, L., Burns, A. G., et al. (2014). The NCAR TIE-GCM: A community model of the coupled thermosphere/ionosphere system. In J. Huba, R. Schunk, & G. Khazanov (Eds.), Eds., *Modeling the ionosphere-thermosphere system*, (p. 201). AGU Geophysical Monograph Series. https://doi.org/10.1002/9781118704417.ch7
5. Kasahara, A. (1974). Various vertical coordinate systems used for numerical weather prediction. *Monthly Weather Review*, **102**(7), 509–522. https://doi.org/1520-0493(1974)102<0509:VVCSUF>2.0.CO;2
6. Hsu, V. W. (2016). *An Indirect and Dynamically Induced Energy Mechanism in a Plasma- Neutral Atmosphere* (Doctoral dissertation, University of Colorado at Boulder).

Acknowledgements

This work is based upon work supported by the National Science Foundation Graduate Research Fellowship under Grant DGE 2040434,, the NASA GDC IDS under Contract No. 80GSFC22CA012, and the NASA Heliophysics Division Space Weather Science Application Initiative under Grant 80NSSC21K1554.